



Northern Illinois
University

Search for Charged Higgs Bosons in the $\tau + \ell$ Final State with 139 fb^{-1} of pp Collision Data at $\sqrt{s} = 13\text{ TeV}$ with the ATLAS Experiment

Dissertation Defense

Elliot Parrish[†]

[†]Northern Illinois University, USA

October 13, 2022

Introduction

Theory

The Standard Model

New Physics

Charged Higgs Bosons

Experimental Apparatus

LHC

ATLAS

Object Reconstruction

Simulation

$$H^\pm \rightarrow \tau^\pm \nu_\tau$$

Background Modeling

MVA

PNN HPO

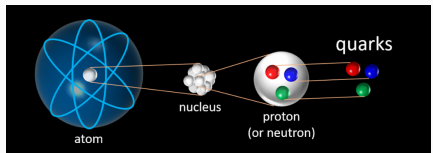
Results

Conclusion

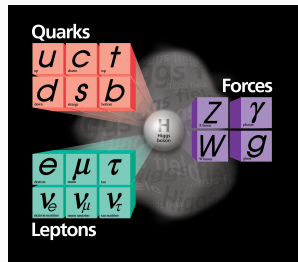
- This defense will take ≈ 1 hour
 - I will walk you through the work that is contained in my PhD dissertation
 - After the presentation is complete, there will be time for public questions, then the committee and I will address comments privately
 - When we are done, I will return, the committee will discuss among themselves then return
- General Guidelines
 - Please remain muted unless you are speaking
 - There will be time at the end for questions, but feel free to interrupt if there is something urgent
- Thank you for attending!

What are we made of?

- The scientific field of particle physics seeks to explain the building blocks of the universe
 - How many fundamental particles are there?
 - How do they interact with each other?
- The Standard Model of Particle Physics (SM)
 - Matter is comprised of fermions
 - Half-integer spin ($s = \frac{1}{2}, \frac{3}{2}, \frac{5}{2}$, etc.)
 - Quarks combine to create hadrons (protons, neutrons, $\pi^{\pm,0}$, etc)
 - Forces are carried by an exchange of bosons
 - Integer spin ($s = 0, 1, 2$, etc.)
 - Gluon (g) → Strong force
 - Photon (γ) → Electromagnetism
 - W^\pm, Z^0 → Weak force

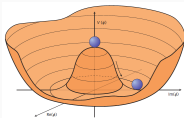


[1] [2]

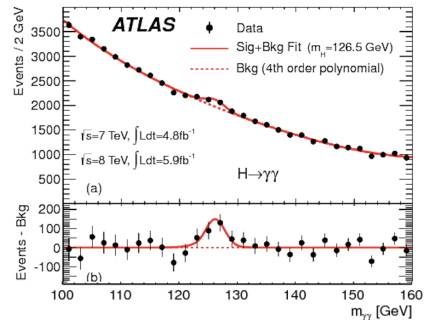


The Higgs Boson

- Theorized by Higgs, Englert, and Brout in 1964
 - Complex scalar doublet ($s = 0$)
 - Non-zero vacuum expectation value
- Interactions with Higgs field give particles mass
- Discovered jointly by the ATLAS and CMS collaborations in 2012



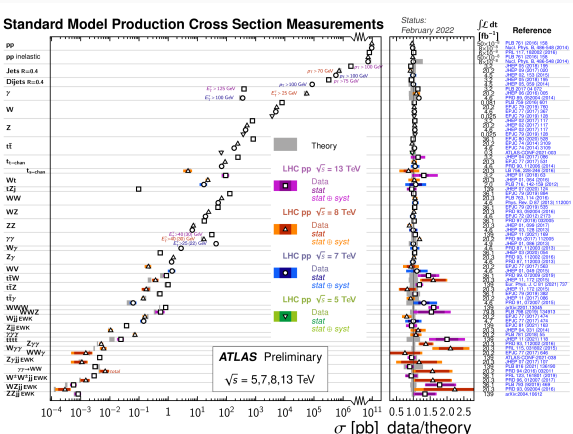
[3]



[4]

The Standard Model

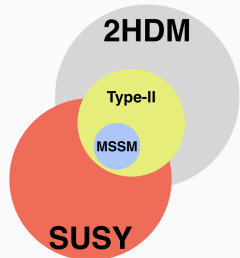
- Predicts the probabilities of creation and decay of particles (among many other things)
 - Has been thoroughly tested
 - Measurements agree to a high degree of accuracy
- Not a complete theory Not a full list
 - Gravity
 - Matter-antimatter asymmetry in the universe
 - Predicted neutrino masses are 0
 - Observed neutrino mixing says otherwise



Beyond the Standard Model



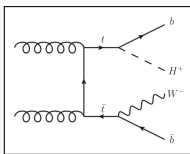
- Hierarchy problem, “unnaturalness”
 - Electroweak scale is ~ 100 GeV
 - Planck scale is $\sim 2.4 \times 10^{18}$ GeV
- 2 Higgs Doublet Models and Supersymmetry (SUSY) are large groups of theories attempting to address these issues
 - 2HDM have two complex doublet scalar fields [5]
 - Two relevant free parameters, $\tan \beta$ and m_{H^\pm}
 - $\tan \beta$ is the ratio of the vacuum expectation values of the two doublets
 - SUSY proposes a symmetry between fermions and bosons
 - Many new possible particles
 - Minimal Supersymmetric Standard Model (MSSM) is the smallest SUSY extension to the SM



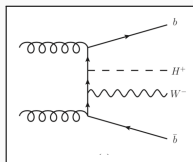
light neutral scalar	h^0
heavy neutral scalar	H^0
neutral pseudoscalar	A^0
two charged scalars	H^\pm

Charged Higgs Bosons

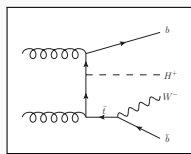
- At the LHC, theoretical production mode of m_{H^\pm} is mainly in top-quark decays or in association with a top-quark (t)
 - H^\pm production mode is dependent on m_{H^\pm}



$$m_{H^\pm} < m_t$$



$$m_{H^\pm} \simeq m_t$$



$$m_{H^\pm} > m_t$$

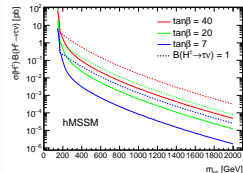
- $H^\pm \rightarrow \tau^\pm \nu_\tau$ decay channel remains significant for high $\tan \beta$
- Two sub-channels based on the decay mode of associated t

$t \rightarrow Wb \rightarrow jets$

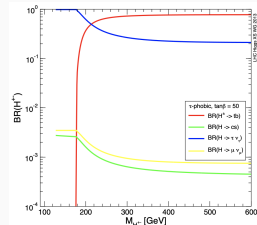
Sensitive at high mass due to higher $W \rightarrow q\bar{q}$ BR

$t \rightarrow Wb \rightarrow \ell$

Theory Charged Higgs Bosons

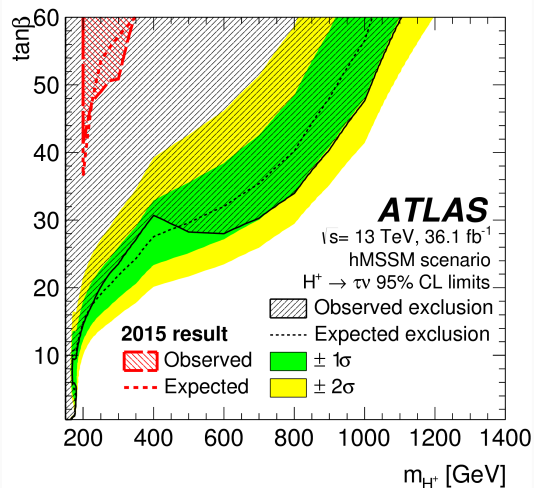
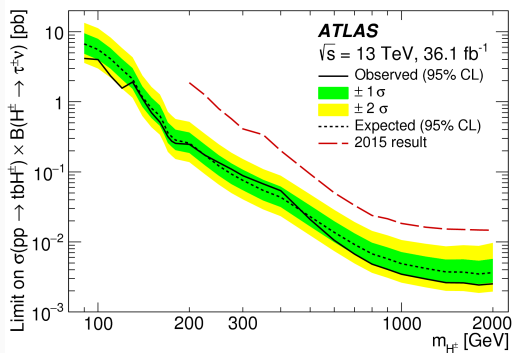


[6]

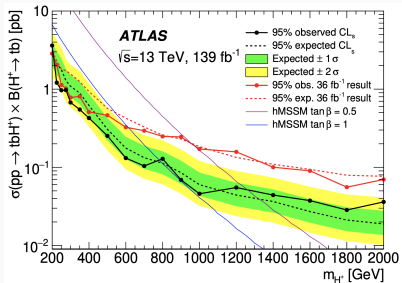


[7]

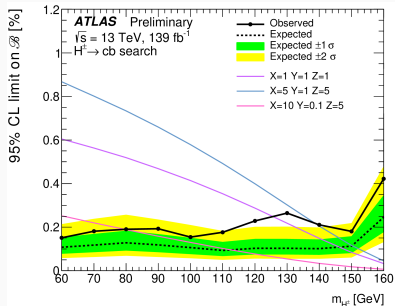
- Previous limits on the production of $H^\pm \rightarrow \tau^\pm \nu_\tau$ and the free parameters $\tan \beta$ and m_{H^\pm}



Other H^\pm Searches



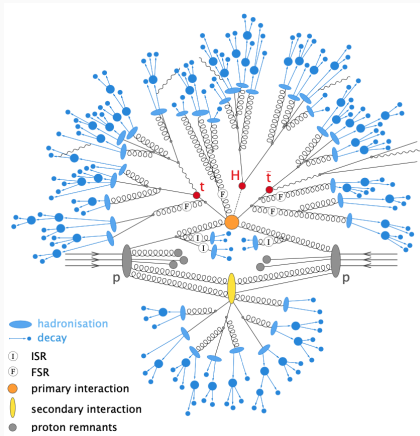
[8]



[9]

Particle Collisions

- Most particles we are interested in are not stable and cannot be observed in our environment
- Collide known particles to study them and potentially new particles
 - $E^2 = m^2 c^4 + p^2 c^2$
- Hadronization
 - Quarks cannot exist on their own
 - Must combine to form bound states
 - Combine shower into a jet



[10]

Large Hadron Collider

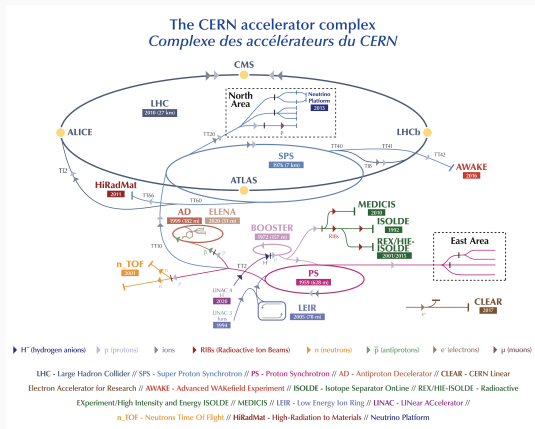


- Largest particle collider ever built
- Highest energy particle collider
- Located at CERN outside of Geneva, Switzerland
- Four main collision points
 - **ATLAS**, ALICE, CMS, LHCb

Selected Run-2 LHC Parameters

Circumference	26,659 m
Magnet operating temperature	1.9 K
Beam energy	6.5 TeV (13 CM TeV)
Protons per bunch	1.2×10^{11}
Bunches per beam	2808
Speed of bunches	> 1,000,000,000 km/hr ($\simeq 99.999\% c$)

[11]

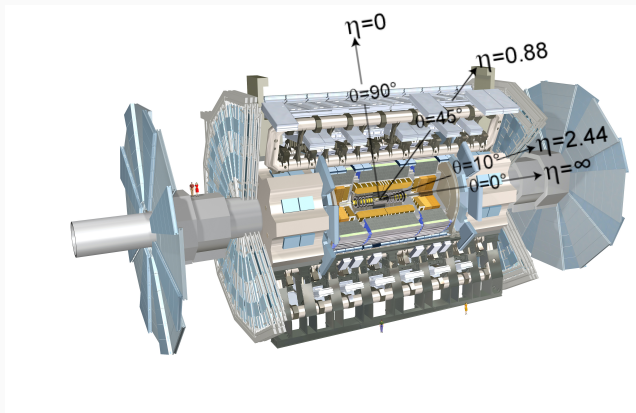


[12]

The ATLAS Detector



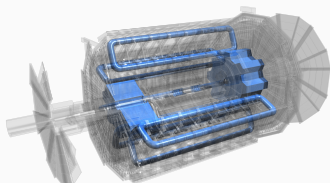
- General purpose particle detector
 - Magnet System
 - Tracker
 - Calorimeters
 - Muon Spectrometer
- Coordinate system origin at interaction point
 - r is radial distance
 - $\eta \equiv -\ln(\tan(\frac{\theta}{2}))$
 - ϕ is azimuthal angle



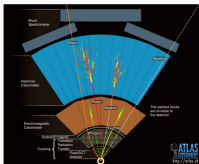
Magnet System and Inner Detector



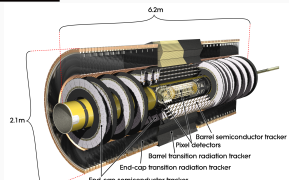
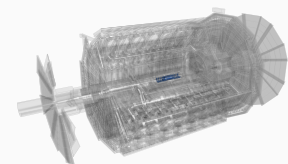
- Central solenoid
 - 2 T magnetic field
 - Bends charged particles in transverse plane
- Toroid system
 - 3.9 T magnetic field
 - Bends charged particles (μ) along beam axis



- Inner-detector (ID)
 - Tracks trajectories of charged particles
 - Used to measure momentum in the transverse plane (p_T)

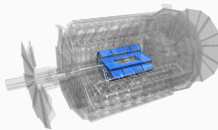
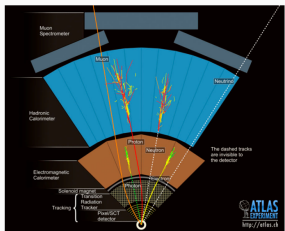


[13]

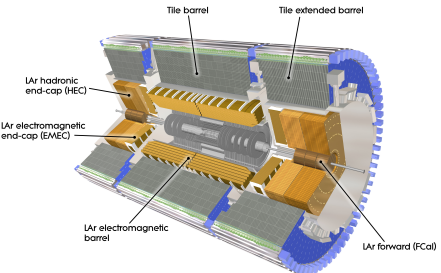


Calorimeters

- Important in jet, τ , E_T^{miss} and μ identification and triggering
- Measure energy of charged particles
 - Designed to fully absorb particles



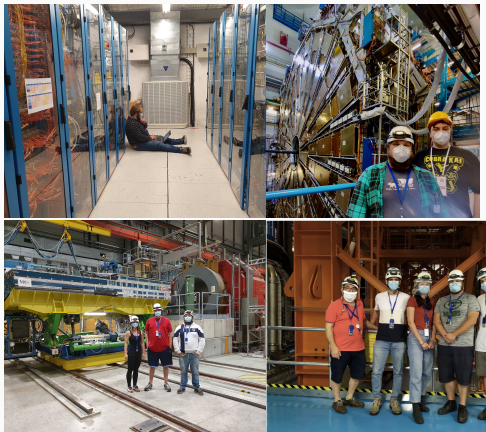
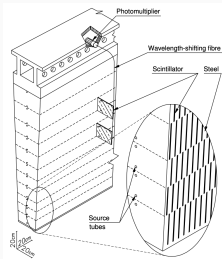
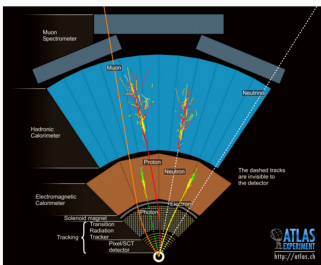
[13]



Tile Calorimeter



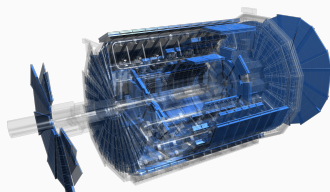
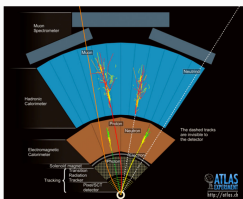
- Scintillating tile with steel absorber
- I served as Data Quality Co-Coordinator for several years
 - In Run-2 99.65% DQ efficiency [15]



Muon System and Trigger



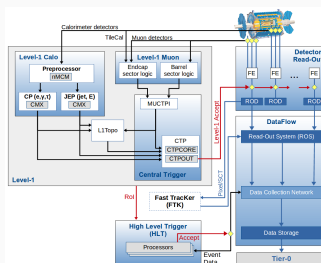
- Muon Spectrometers (MS) detect and measure μ
 - Muons are minimally ionizing
 - μ reach the outermost region of the detector
 - Information combined with inner detector to reconstruct μ



Search for $H^\pm \rightarrow \tau^\pm \nu_\tau$ with ATLAS

Trigger System

- Need to quickly sort through data and decide if a collision is interesting or not
- Mix of hardware and software



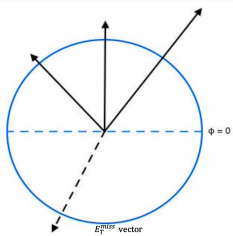
[17]

Experimental Apparatus ATLAS

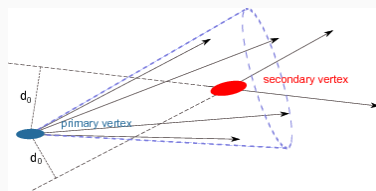
Reconstruction: E_T^{miss} and b -jets



- Particles like ν do not leave a signature within ATLAS
- Instead, infer their presence through momentum conservation
 - Negative vector sum of all objects in a collision event



- b quark initiated hadronic showers are identified by a displaced vertex, etc.
- Reconstructed as a jet, tagged as a b -jet
 - Algorithms designed to identify b -jets called taggers [18]

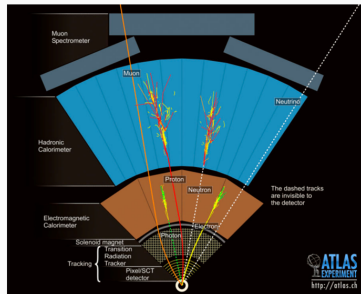


[19]

Reconstruction: e and μ

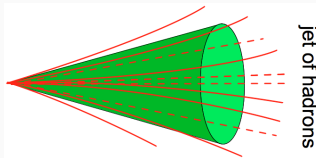
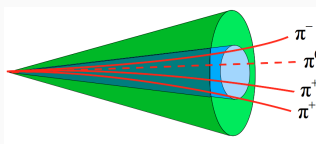


- Electron identification
 - Information from the ID and showers in the EM calorimeter are combined
 - This analysis uses tight ID and tight isolation requirements
- μ identification
 - Information from the ID is combined with the MS
 - This analysis uses tight ID and tight isolation requirements



Reconstruction: τ leptons

- τ leptons typically decay before they interact with the detector
- τ leptons decay hadronically $\approx 65\%$ of the time
 - leptonic decays are not considered
- Number of charged hadrons (π^\pm) in decays defines number of prongs
 - 1 π^\pm occurs 72% of the time
 - 3 π^\pm occurs 22% of the time
 - Of these decays, 68% contain $> 1 \pi^0$
- ν_τ are also produced in these decays, only visible part of τ can be reconstructed

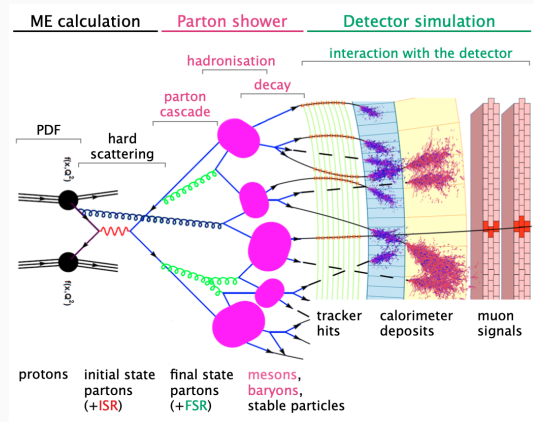


jet of hadrons

[20]

Simulation

- Incredibly detailed simulations are used to create analysis strategy
 - Entire data flow from collision to detector readout is simulated
 - Many different options to generate simulations
 - Some excel at specific tasks and not great at others
- Control regions are used to verify simulation agreement with data



[10]

Analysis Overview

- Search for singly charged H^\pm decaying to $\tau^\pm \nu_\tau$ over a wide mass range
 - Low mass ($m_{H^\pm} < m_t$):
 - Intermediate mass* ($m_{H^\pm} \simeq m_t$)
 - High mass ($m_{H^\pm} > m_t$)

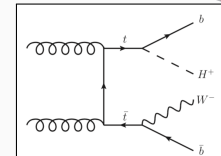
- Dominant backgrounds

Backgrounds w/ prompt hadronic τ	Backgrounds w/ fake τ
$t\bar{t}$ estimated with simulation	Fake $j \rightarrow \tau$ estimated with data driven fake factor method
$V + jets$ estimated with simulation	Fake $\ell \rightarrow \tau$ estimated with simulation, validated on $Z \rightarrow ee$
VV estimated with simulation	

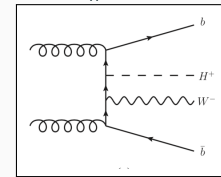
- MVA score is used as the final discriminant

Sub-Channel							
$\tau + jets$ SR	E_T^{miss} Trigger	1 hadronic τ $p_T^\tau > 40$ GeV	0 ℓ (e or μ) $p_T^\ell > 20$ GeV	≥ 3 jets $p_T^j > 25$ GeV	≥ 1 b-jets $p_T^{b-jet} > 25$ GeV	$E_T^{\text{miss}} > 150$ GeV	$m_T(\tau, E_T^{\text{miss}}) > 50$ GeV
$\tau + \ell$ SR	Single Lepton Trigger	1 hadronic τ $p_T^\tau > 30$ GeV	1 ℓ (e or μ) $p_T^\ell > 30$ GeV	≥ 1 jet $p_T^j > 25$ GeV	≥ 1 b-jets $p_T^{b-jet} > 25$ GeV	$E_T^{\text{miss}} > 50$ GeV	Opposite sign τ and ℓ

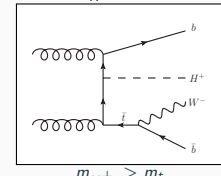
*: First time probed experimentally JHEP 09(2018)139



$$m_{H^\pm} < m_t$$



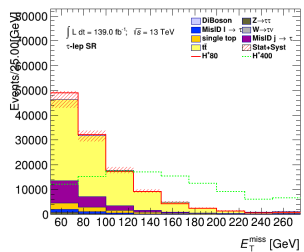
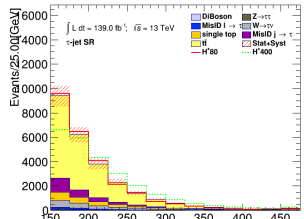
$$m_{H^\pm} \simeq m_t$$



$$m_{H^\pm} > m_t$$

Background Estimation

- Signal region E_T^{miss} distributions on right show background composition
- Define control regions to verify main sources of background

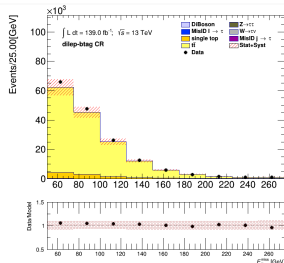
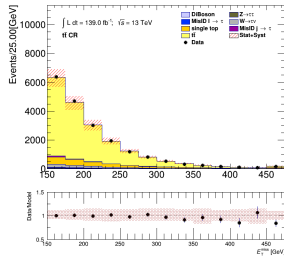


Background Estimation

- Signal region E_T^{miss} distributions on right show background composition
- Define control regions to verify main sources of background

Background Modeling	$\tau + \text{jets}$	Control Regions	$\tau + \ell$ Control Regions	Data/Model Agreement
$t\bar{t} + \text{single top}$	$t\bar{t}$	Dilepton-btag		✓

- Estimated with simulation

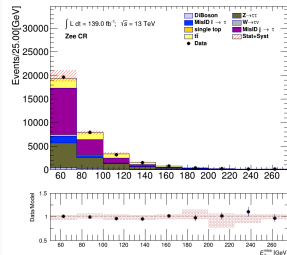
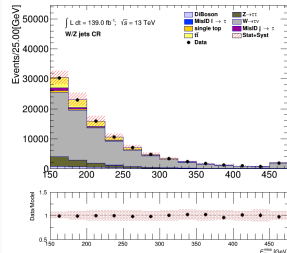


Background Estimation

- Signal region E_T^{miss} distributions on right show background composition
- Define control regions to verify main sources of background

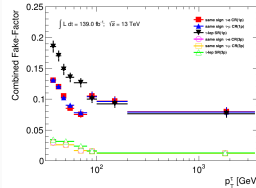
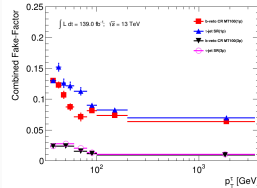
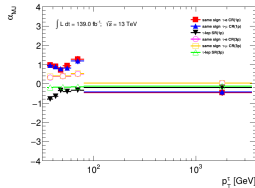
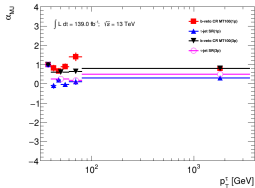
Background Modeling	$\tau + \text{jets}$	Control Regions	$\tau + \ell$ Control Regions	Data/Model Agreement
$t\bar{t} + \text{single top}$	$t\bar{t}$	Dilepton-btag	✓	
V+Jets	W+Jets	Zee (Fake $\ell \rightarrow \tau$ enriched)	✓	

- Estimated with simulation



Background Estimation: $j \rightarrow \tau$ Fakes

- $j \rightarrow \tau$ fakes estimated with a data-driven fake factor (FF) method (from QCD-like Multijet and $W+jets$)
 - Anti-selection of τ that fail τ ID but pass looser selection
 - Define CRs to extract fake factors
 - Subtract SM contribution from simulation
 - $FF = \frac{N_{fake\tau}}{N_{anti-\tau}}$
- In SR, measure fraction of fakes (α) using template fit of τ ID RNN score distributions using template shapes from $anti - \tau$ distributions in CRs
- $FF_{sig} = \alpha_{MJ} \times FF_{MJ} + (1 - \alpha_{MJ}) \times FF_{W+jets}$
- In SR, $N_{fake\tau} = FF_{sig} \times N_{anti-\tau}$

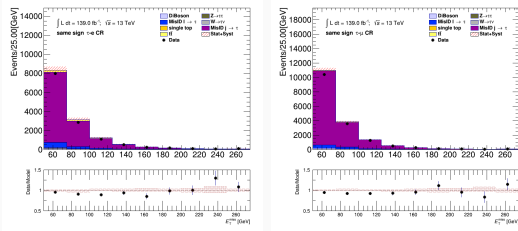
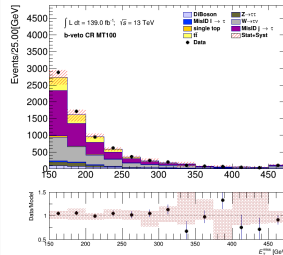


Background Estimation: $j \rightarrow \tau$ Fakes

- Signal region E_T^{miss} distributions on right show background composition
- Define control regions to verify main sources of background

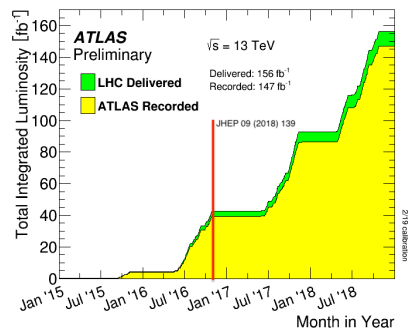
Background Modeling	$\tau + \text{jets}$ Control Regions	$\tau + \ell$ Control Regions	Data/Model Agreement
$t\bar{t} + \text{single top}$	$t\bar{t}$	Dilepton-btag	✓
Fake $j \rightarrow \tau$ enriched	b veto $m_T(\tau, E_T^{\text{miss}}) > 100$	Same Sign	✓

- Estimated with a data-driven fake factor method



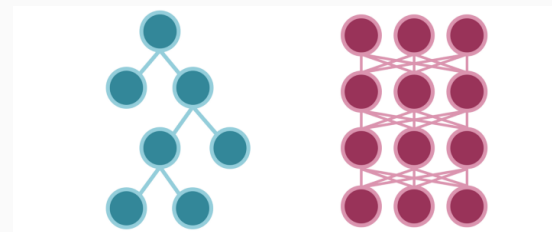
Updates to analysis since last publication

- Signal mass range extended
 - Previous: $90 \leq m_{H^\pm} \leq 2000$ GeV
 - Current: $80 \leq m_{H^\pm} \leq 3000$ GeV
- Increased statistics of signal due to optimized simulation generation
- New analysis framework centered around using modern Machine Learning tools
- Investigated new multivariate analysis techniques
- Improved particle identification algorithms
- Almost 4× more data



[21]

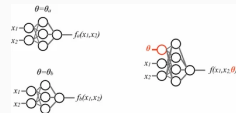
- Boosted Decision Tree (BDT)
 - Cascading decisions bin parameter space to optimize accuracy
 - Deterministic approach
 - Excel at exploiting linear correlations
 - Often combined into a random forest



- Neural Networks
 - Network of connected nodes of activation functions connected by weights
 - Probabilistic approach
 - Excel at exploiting non-linear correlations

Parameterized Neural Networks

- Parameterized Neural Networks (PNNs) can be trained and evaluated on entire m_{H^\pm} range
 - One model for entire mass range makes analysis less computationally expensive
 - PNN can be evaluated on mass points that are not simulated
 - Detailed information here: [arXiv:1601.07913](https://arxiv.org/abs/1601.07913)
- Background modeling and classifier training kept statistically independent via the k-fold method ($k = 5$)
- Trained using simulation for backgrounds with true τ
 - Separate models trained on 1 prong and 3 prong τ
 - τ polarization used to enhance low m_{H^\pm} performance
 - $\Upsilon = \frac{E_T^{\pi^\pm} - E_T^{\pi^0}}{E_T^\tau} \approx 2 \frac{p_T^{\tau\text{-track}}}{p_T^\tau} - 1$
 - $\tau + \ell$ channel is trained inclusive for $\tau + e$ and $\tau + \mu$



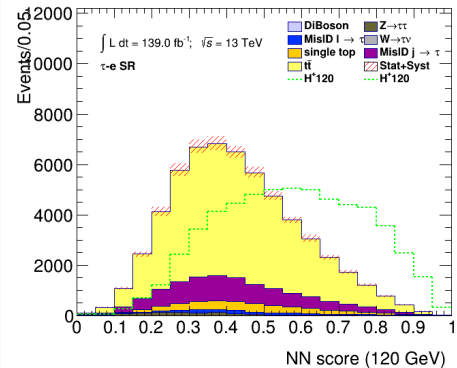
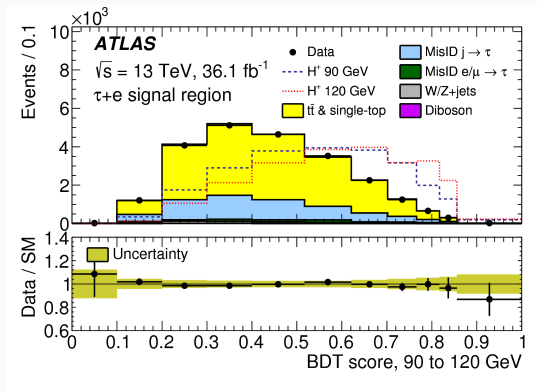
[23]

	Fold 1	Fold 2	Fold 3	Fold 4	Fold 5	Background
Partition 1	Evaluation	Train	Train	Train	Train	Fold 1
Partition 2	Train	Evaluation	Train	Train	Train	Fold 2
Partition 3	Train	Train	Evaluation	Train	Train	Fold 3
Partition 4	Train	Train	Train	Evaluation	Train	Fold 4
Partition 5	Train	Train	Train	Train	Evaluation	Fold 5

$\tau + \ell$ Input Variables		
p_T^τ	η^τ	ϕ^τ
p_T^ℓ	η^ℓ	ϕ^ℓ
$p_T^{j_0}$	η^{j_0}	ϕ^{j_0}
E_T^{miss}	$\phi^{E_T^{\text{miss}}}$	p_T^h
$m_{Truth}^{H^\pm}$	Υ^τ	

$\tau + \text{jets}$ Input Variables		
p_T^τ	η^τ	ϕ^τ
$p_T^{j_0}$	η^{j_0}	ϕ^{j_0}
$p_T^{j_1}$	η^{j_1}	ϕ^{j_1}
$p_T^{j_2}$	η^{j_2}	ϕ^{j_2}
E_T^{miss}	$\phi^{E_T^{\text{miss}}}$	$m_{Truth}^{H^\pm}$
Υ^τ		

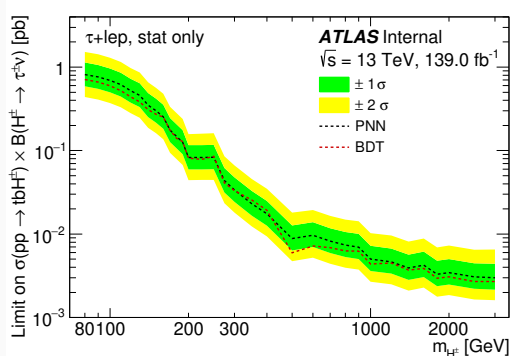
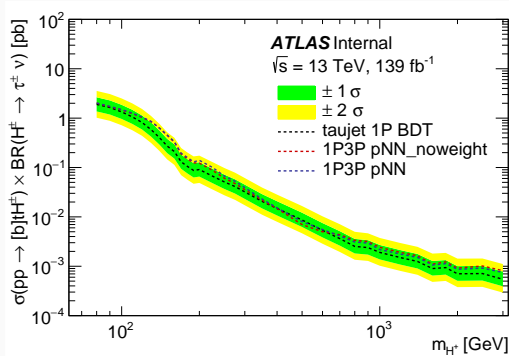
Boosted Decision Tree vs Parameterized Neural Network



Boosted Decision Tree vs Parameterized Neural Network



- These comparisons were done with an optimized BDT and an unoptimized PNN
- PNN chosen as classifier



PNN Input Variable Selection



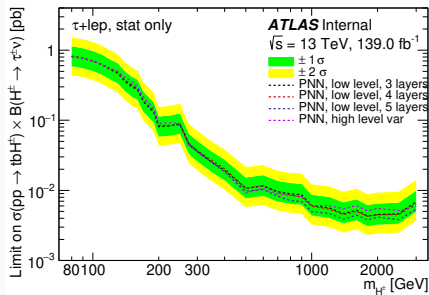
Low Level Input Variables

p_T^τ	η^τ	ϕ^τ
p_T^ℓ	η^ℓ	ϕ^ℓ
p_T^{b-jet}	η^{b-jet}	ϕ^{b-jet}
p_T^{jet}	η^{jet}	ϕ^{jet}
E_T^{miss}	ϕ_E^{miss}	p_T^h
Υ	$m_{H^\pm}^{\text{Truth}}$	

High Level Input Variables

p_T^τ	p_T^{b-jet}	p_T^ℓ
E_T^{miss}	$\Delta\phi_{\tau, \text{miss}}$	$\Delta\phi_{b-jet, \text{miss}}$
$\Delta\phi_{\ell, \text{miss}}$	$\Delta R_{\tau, \ell}$	$\Delta R_{b-jet, \ell}$
$\Delta R_{b-jet, \tau}$	$\Delta\phi_{\tau, \text{miss}}/\Delta\phi_{jet, \text{miss}}$	Υ
$m_{H^\pm}^{\text{Truth}}$		

- Comparison between raw input variables and engineered variables
- Expected limits in the $\tau + \ell$ subchannel was used as figure of merit
- Low level variables best at high m_{H^\pm}



- Performed in the $\tau + \ell$ sub-channel
- Used area under curve (AUC) of scores as figure of merit
 - Averaged over 5 kfolds, standard deviation is taken from kfolds
 - Average Area Under the Curve (AUC) from 80 GeV to 500 GeV to optimize for low mass
- Used early stopping for training
 - $\Delta_{min} = 0.00001$ and a patience of 10
 - Best weights were kept
- To speed up hyperparameter optimization (HPO), ran multiple small grids of hyperparameters
 - Scan over activation functions and loss functions
 - Scan over dropout value
 - Scan over activation function
 - Scan over LeakyReLU α
 - Fixed alpha over more widths and depths

- LeakyReLU activation function has an α parameter
- Slope of negative portion
 - Prevents neurons from “dying” by allowing negative weight values
- Standard relu is where $\alpha = 0$



PNN Hyperparameter Optimization



Parameter	softsign	relu	LeakyReLU
activation function	softsign	relu	LeakyReLU
loss function	binary crossentropy	mean squared error	mean absolute error
width	32		
depth	10		

PNN Hyperparameter Optimization



Parameter			
activation function	softsign	relu	LeakyReLU
loss function	binary crossentropy	mean squared error	mean absolute error
width	32		
depth	10		

Parameter			
width	8	16	32
depth	3	5	10
dropout	0.1	0.3	
activation function	softsign		
loss function	binary crossentropy		

PNN Hyperparameter Optimization



Parameter			
activation function	softsign	relu	LeakyReLU
loss function	binary crossentropy	mean squared error	mean absolute error
width	32		
depth	10		

Parameter			
width	8	16	32
depth	3	5	10
dropout	0.1	0.3	
activation function	softsign		
loss function	binary crossentropy		

Parameter			
width	32	64	128
depth	2	3	4
dropout	0.1		
activation function	softsign	relu	LeakyReLU
batch size	1025		
loss function	binary crossentropy		

PNN Hyperparameter Optimization



Parameter	softsign	relu	LeakyReLU
activation function	softsign	relu	LeakyReLU
loss function	binary crossentropy	mean squared error	mean absolute error
width	32		
depth	10		

Parameter	width	8	16	32
width	8	16	32	
depth	3	5	10	
dropout	0.1	0.3		
activation function	softsign			
loss function	binary crossentropy			

Parameter	width	32	64	128
width	32	64	128	
depth	2	3	4	
dropout	0.1			
activation function	softsign	relu	LeakyReLU	
batch size	1025			
loss function	binary crossentropy			

Parameter	width	32	64	128	
width	32	64	128		
depth	2	3	4		
α	0.01	0.05	0.001	0.005	
batch size	1024				
dropout	0.1				
activation function	LeakyReLU				
loss function	binary crossentropy				

PNN Hyperparameter Optimization



Parameter			
activation function	softsign	relu	LeakyReLU
loss function	binary crossentropy	mean squared error	mean absolute error
width	32		
depth	10		

Parameter			
width	8	16	32
depth	3	5	10
dropout	0.1	0.3	
activation function	softsign		
loss function	binary crossentropy		

Parameter			
width	32	64	128
depth	2	3	4
dropout	0.1		
activation function	softsign	relu	LeakyReLU
batch size	1025		
loss function	binary crossentropy		

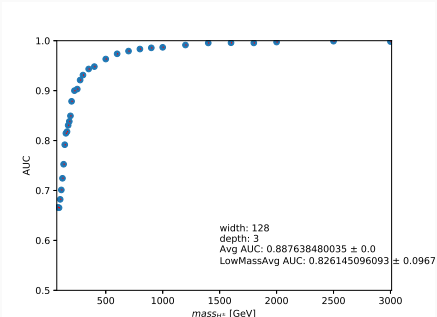
Parameter				
width	32	64	128	
depth	2	3	4	
α	0.01	0.05	0.001	0.005
batch size	1024			
dropout	0.1			
activation function	LeakyReLU			
loss function	binary crossentropy			

Parameter				
width	32	64	128	256
depth	2	3	4	5
batch size	1024			
dropout	0.1			
activation function	LeakyReLU			
α	0.05			
loss function	binary crossentropy			

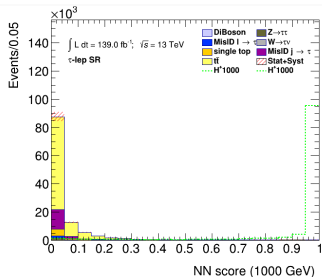
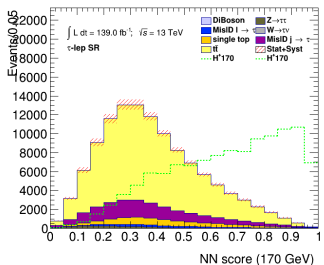
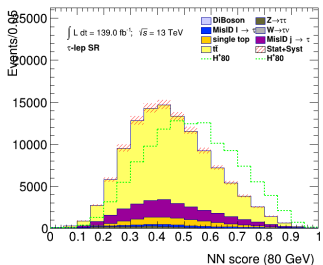
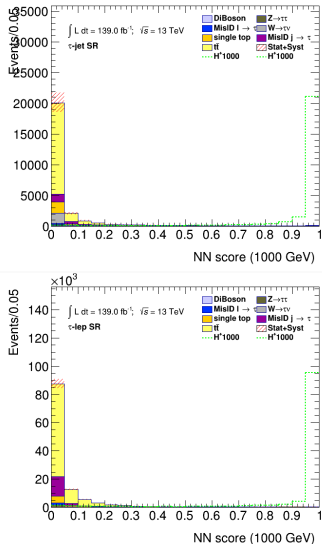
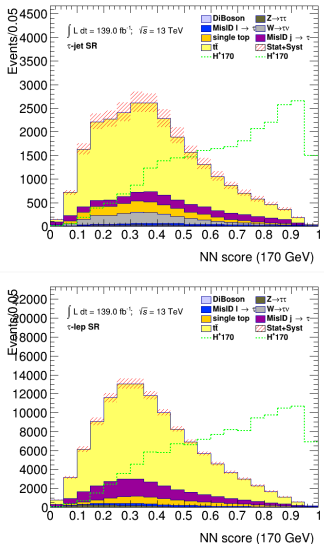
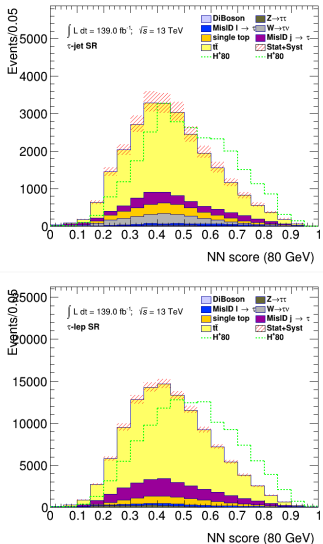
Final PNN Model Performance



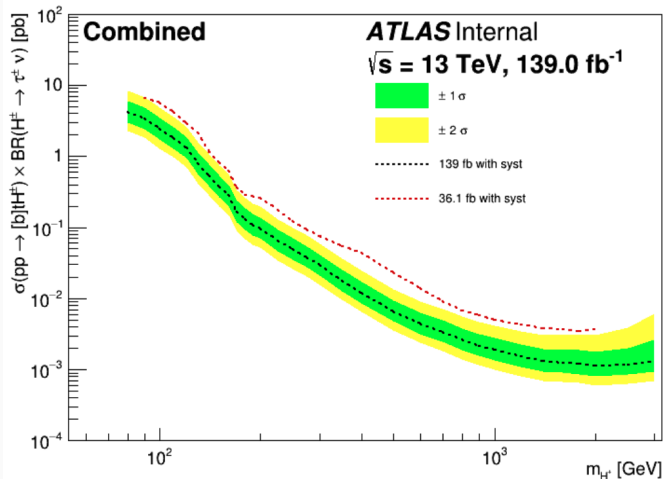
width	depth	Avg	LowMassAvg
128	3	0.8876 ± 0.0000	0.8261 ± 0.0968
128	5	0.8861 ± 0.0000	0.8235 ± 0.1000
128	4	0.8858 ± 0.0000	0.8232 ± 0.0994
128	2	0.8857 ± 0.0000	0.8231 ± 0.1006
64	4	0.8857 ± 0.0002	0.8230 ± 0.0994
64	2	0.8855 ± 0.0004	0.8228 ± 0.0996
64	5	0.8853 ± 0.0005	0.8224 ± 0.0997
64	3	0.8853 ± 0.0011	0.8223 ± 0.0994
256	5	0.8844 ± 0.0002	0.8213 ± 0.1003
256	4	0.8823 ± 0.0000	0.8181 ± 0.1013
32	3	0.8798 ± 0.0012	0.8139 ± 0.1031
32	4	0.8799 ± 0.0009	0.8139 ± 0.1031
32	2	0.8796 ± 0.0004	0.8135 ± 0.1023
32	5	0.8792 ± 0.0011	0.8128 ± 0.1035
256	2	0.8781 ± 0.0002	0.8120 ± 0.1023



PNN Results



$H^\pm \rightarrow \tau\nu$ Expected Limits

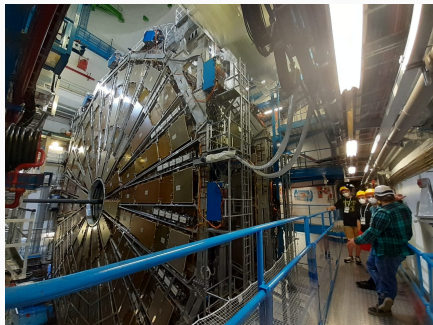


Combined $\tau + \text{jets}$ and $\tau + \ell$ signal regions

Conclusions



- A search for $H^\pm \rightarrow \tau^\pm \nu_\tau$ was improved upon
- Investigated, optimized, and implemented modern machine learning techniques
- New analysis strategy outperforms previous analysis by $\gtrsim 3\times$
- Analysis is still blinded and work is ongoing towards a publication



Thank You



References i

- [1] D. Hemphill, *The behavior of the primordial universe*, Apr. 2020. [Online]. Available:
https://www.physics.purdue.edu/about/prizes_awards/charlotte_ida_litman_tubis_award/2017_behavior_primordial_universe.html.
- [2] D. Leah, *The standard model: The most successful theory ever*, [Online]. Available: <https://news.fnal.gov/2011/11/the-standard-model-the-most-successful-theory-ever/>.
- [3] J. Ellis, “Higgs Physics,” 117–168. 52 p, Dec. 2013, 52 pages, 45 figures, Lectures presented at the ESHEP 2013 School of High-Energy Physics, to appear as part of the proceedings in a CERN Yellow Report. DOI: 10.5170/CERN-2015-004.117. arXiv: 1312.5672. [Online]. Available: <https://cds.cern.ch/record/1638469>.

References ii

- [4] ATLAS Collaboration, "Observation of a new particle in the search for the standard model higgs boson with the atlas detector at the lhc," *Physics Letters B*, vol. 716, no. 1, pp. 1–29, 2012.
- [5] G. Branco, P. Ferreira, L. Lavoura, M. Rebelo, M. Sher, and J. P. Silva, "Theory and phenomenology of two-higgs-doublet models," *Physics Reports*, vol. 516, no. 1–2, pp. 1–102, Jul. 2012, ISSN: 0370-1573. DOI: 10.1016/j.physrep.2012.02.002. [Online]. Available: <http://dx.doi.org/10.1016/j.physrep.2012.02.002>.
- [6] The ATLAS Collaboration, "Search for charged Higgs bosons decaying via $H^\pm \rightarrow \tau^\pm \nu_\tau$ in the $\tau + \text{jets}$ and $\tau + \text{lepton}$ final states with 36 fb^{-1} of pp collision data recorded at $\sqrt{s} = 13 \text{ TeV}$ with the ATLAS experiment," *JHEP*, vol. 09, p. 139, 2018. DOI: 10.1007/JHEP09(2018)139. arXiv: 1807.07915 [hep-ex].

References iii

- [7] C. T. e. a. Potter, *Handbook of lhc higgs cross sections: 3. higgs properties: Report of the lhc higgs cross section working group*, en, 2013. DOI: 10.5170/CERN-2013-004. [Online]. Available: <http://cds.cern.ch/record/1559921>.
- [8] ATLAS collaboration, “Search for charged higgs bosons decaying into a top quark and a bottom quark at $\sqrt{s} = 13$ tev with the atlas detector,” *Journal of High Energy Physics*, vol. 2021, no. 6, p. 145, 2021. DOI: 10.1007/JHEP06(2021)145. [Online]. Available: [https://doi.org/10.1007/JHEP06\(2021\)145](https://doi.org/10.1007/JHEP06(2021)145).

- [9] “Search for a light charged Higgs boson in $t \rightarrow H^+ b$ decays, with $H^+ \rightarrow cb$, in the lepton+jets final state in proton-proton collisions at $\sqrt{s} = 13$ TeV with the ATLAS detector,” CERN, Geneva, Tech. Rep., 2021, All figures including auxiliary figures are available at
<https://atlas.web.cern.ch/Atlas/GROUPS/PHYSICS/CONFNOTES/ATLAS-CONF-2021-037>. [Online]. Available: <https://cds.cern.ch/record/2779169>.
- [10] C. Wanotayaroj, “Search for a Scalar Partner of the Top Quark in the Jets+MET Final State with the ATLAS detector,” Presented 25 Oct 2016, Nov. 2016. [Online]. Available: <http://cds.cern.ch/record/2242196>.
- [11] CERN, *Facts and figures about the lhc*, [Online]. Available:
<https://home.cern/resources/faqs/facts-and-figures-about-lhc>.

References v

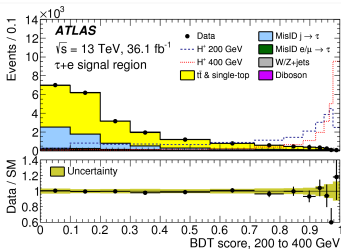
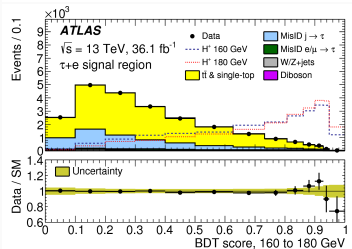
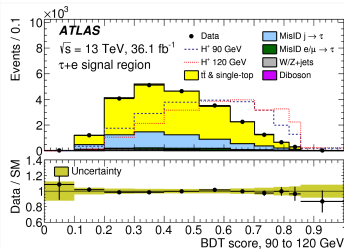
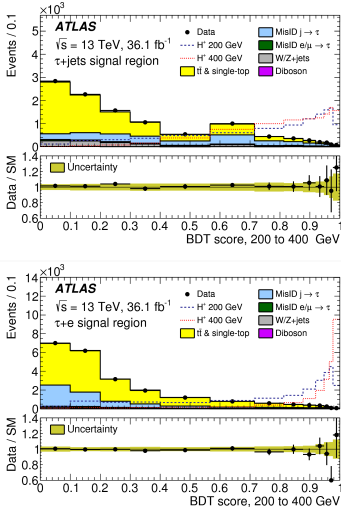
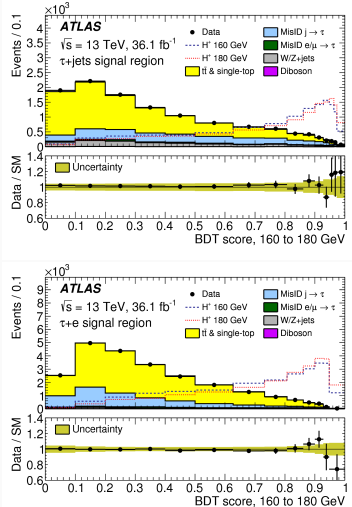
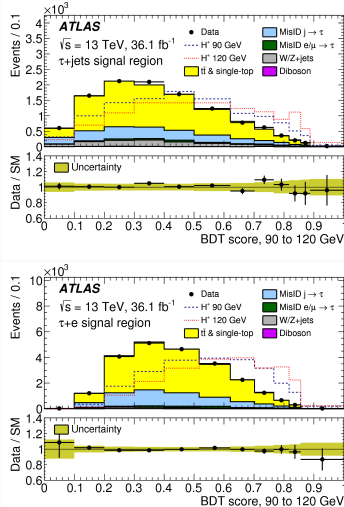
- [12] E. Lopienska, “The CERN accelerator complex, layout in 2022. Complexe des accélérateurs du CERN en janvier 2022,”, Feb. 2022, General Photo. [Online]. Available: <https://cds.cern.ch/record/2800984>.
- [13] ATLAS Collaboration, *Atlas schematics*, [Online]. Available: <https://atlas.cern/Resources/Schematics>.
- [14] *Pseudorapidity*. Wikipedia, Feb. 2009. [Online]. Available: <https://en.wikipedia.org/wiki/File:Pseudorapidity2.png>.
- [15] ——, “ATLAS data quality operations and performance for 2015–2018 data-taking,” *Journal of Instrumentation*, vol. 15, no. 04, P04003–P04003, Apr. 2020. DOI: 10.1088/1748-0221/15/04/p04003. [Online]. Available: <https://doi.org/10.1088/1748-0221/15/04/p04003>.

- [16] ——, *ATLAS tile calorimeter: Technical Design Report*, ser. Technical design report. ATLAS. Geneva: CERN, 1996. DOI: 10.17181/CERN.JRBJ.7028. [Online]. Available: <https://cds.cern.ch/record/331062>.
- [17] ——, *Atlas daq approved plots*, [Online]. Available: <https://twiki.cern.ch/twiki/bin/view/AtlasPublic/ApprovedPlotsDAQ>.
- [18] ——, “Optimisation and performance studies of the ATLAS b -tagging algorithms for the 2017-18 LHC run,”, Jul. 2017, All figures including auxiliary figures are available at <https://atlas.web.cern.ch/Atlas/GROUPS/PHYSICS/PUBNOTES/ATL-PHYS-PUB-2017-013>. [Online]. Available: <http://cds.cern.ch/record/2273281>.

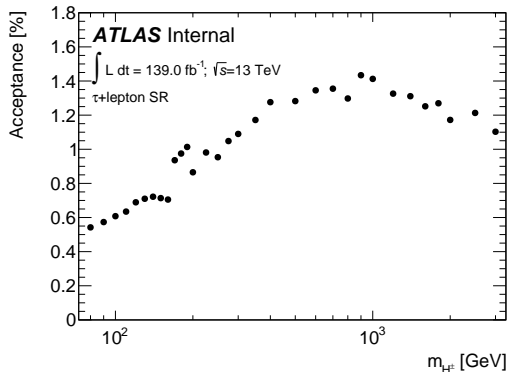
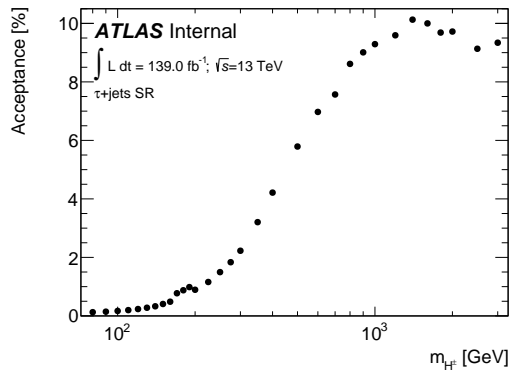
- [19] P. O. Hansson Adrian, “The ATLAS b -jet Trigger,”, Nov. 2011, Comments: 4 pages, 6 figures, conference proceedings for PIC2011. arXiv: 1111.4190. [Online]. Available: <https://cds.cern.ch/record/1397942>.
- [20] Y. Sakurai, “The ATLAS Tau Trigger Performance during LHC Run 1 and Prospects for Run 2,” Tech. Rep., 2014, Comments: LHC Conference 2014. arXiv: 1409.2699. [Online]. Available: <https://cds.cern.ch/record/1754701>.
- [21] ATLAS Collaboration, *Public atlas luminosity results for run-2 of the lhc*, [Online]. Available: https://twiki.cern.ch/twiki/bin/view/AtlasPublic/LuminosityPublicResultsRun2#Integrated_and_Instantaneous_Lum.

- [22] A. Ye, *When and why tree-based models (often) outperform neural networks*, Sep. 2020. [Online]. Available:
<https://towardsdatascience.com/when-and-why-tree-based-models-often-outperform-neural-networks-ceba9ecd0fd8>.
- [23] P. Baldi, K. Cranmer, T. Faucett, P. Sadowski, and D. Whiteson, “Parameterized neural networks for high-energy physics,” *The European Physical Journal C*, vol. 76, no. 5, p. 235, 2016. DOI: 10.1140/epjc/s10052-016-4099-4. [Online]. Available: <https://doi.org/10.1140/epjc/s10052-016-4099-4>.

JHEP 09(2018)139 BDT Scores in Signal Regions



Signal Acceptance

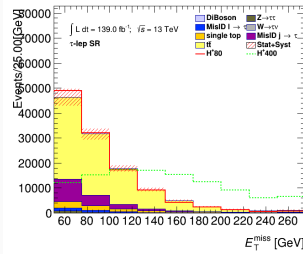
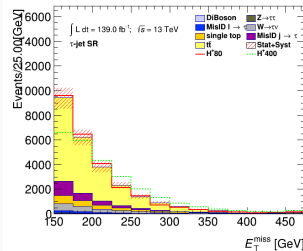


Background Estimation

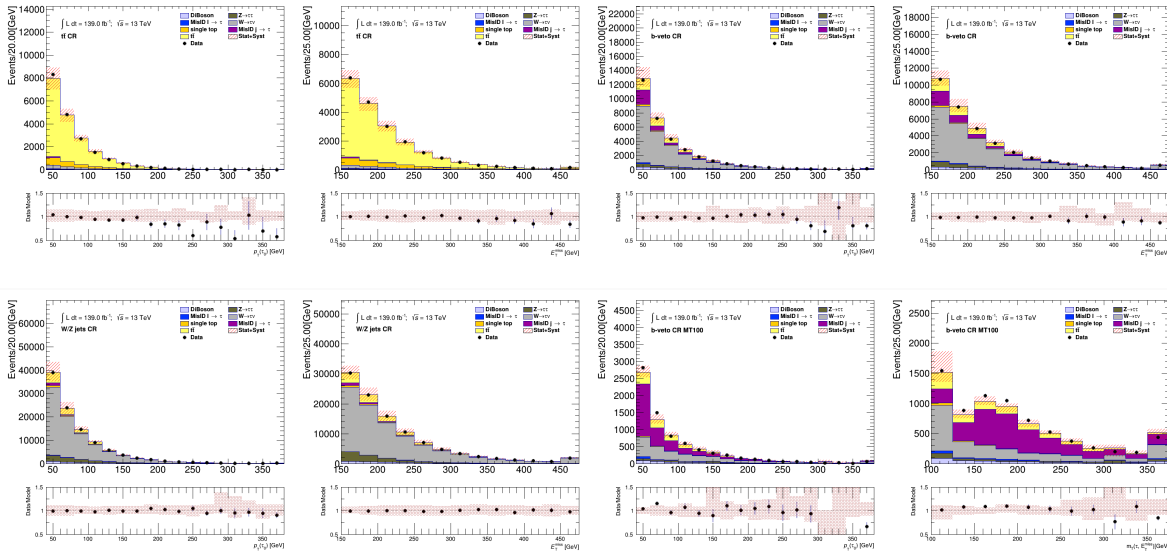
- Control regions defined to verify main sources of background

	$t\bar{t}$ CR	W+Jets CR	b-veto CR	b-veto $m_T > 100$ CR
Number of $\tau_{had-vis}$	1	1	0	0
p_T^τ	> 40 GeV	> 40 GeV	> 40 GeV	> 40 GeV
Number of jets	≥ 3	≥ 3	≥ 3	≥ 3
p_T^{jet}	≥ 25 GeV	≥ 25 GeV	≥ 25 GeV	≥ 25 GeV
Number of b-jets	≥ 2	0	0	0
Number of ℓ	0	0	0	0
E_T^{miss}	> 150 GeV	> 150 GeV	> 150 GeV	> 150 GeV
$m_T(\tau, E_T^{\text{miss}})$	< 100 GeV	< 100 GeV	> 50 GeV	> 100 GeV
Type of modeling	$t\bar{t}$	W+Jets	Close to SR	Fake $j \rightarrow \tau$ enriched

	Dilepton-btag CR	Zee CR	b-veto CR	Same Sign CR
Number of $\tau_{had-vis}$	0	1	0	0
p_T^τ	> 30 GeV	> 30 GeV	> 30 GeV	> 30 GeV
Number of jets	≥ 1	≥ 1	≥ 1	≥ 1
p_T^{jet}	≥ 25 GeV	≥ 25 GeV	≥ 25 GeV	≥ 25 GeV
Number of b-jets	≥ 1	0	0	≥ 1
Number of ℓ	2 (1 e, 1 μ)	1 e	1 tight e (μ)	1 tight e (μ)
E_T^{miss}	> 50 GeV	> 50 GeV	> 50 GeV	> 50 GeV
mass(τ, e)	N/A	> 40; < 140 GeV	N/A	N/A
Type of modeling	$t\bar{t}$ and single-top	Fake $\ell \rightarrow \tau$ enriched	Close to SR	Fake $j \rightarrow \tau$ enriched



$\tau + \text{jets}$ Background Modeling



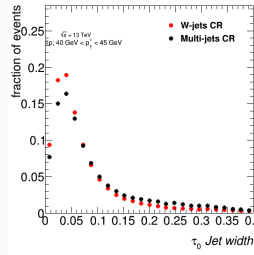
Background Estimation: $j \rightarrow \tau$ Fakes

- Extract Fake-Factors $FF = \frac{N_{\tau_{had-vis}}^{CR}}{N_{\bar{\tau}_{had-vis}}^{CR}}$ from two orthogonal control regions:

Multi-Jet (gluon enriched)	W+Jets (quark enriched)
E_T^{miss} or Multi-Jet trigger	Single lepton triggers
$\geq 1\tau_{had}, p_T^{\tau} > 30 \text{ GeV}$	$\geq 1\tau_{had}, p_T^{\tau} > 30 \text{ GeV}$
≥ 3 jets	≥ 1 jet
0 b-jets	0 b-jets

- Combine the two Fake-Factors via the template fit method:
 - Find two separate templates for anti- τ in each CR
 - Fit both templates to the shape of the anti- τ in the SR
 - Lowest χ^2 of the fit defines α_{MJ} value and the corresponding error
- Number of events with fake τ in the signal region is given by:

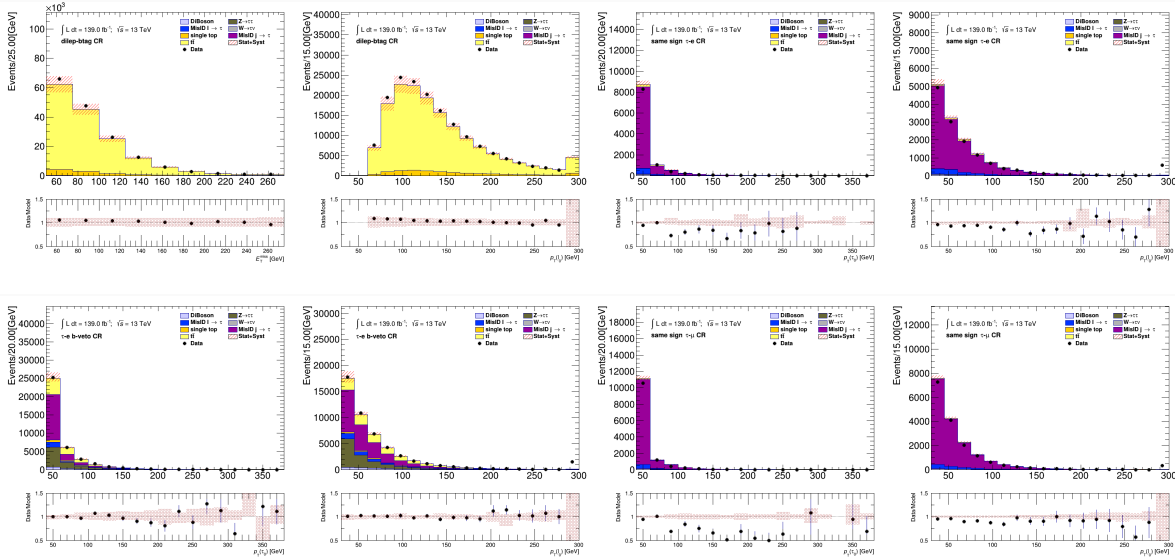
$$N_{fakes}^{Thad-vis} = \sum_i N_{\bar{\tau}_{had-vis}}^{SRi} FF_i$$



- $\bar{\tau}_0$ jet width used in α fitting of 1-prong and 3-prong $\bar{\tau}$

$\bar{\tau} ID$
RNN Score > 0.01
Not loose

$\tau + \ell$ Background Modeling



PNN Hyperparameter Optimization Results

width	depth	80	150	250	500	Avg	LowMassAvg
128	3	0.6661 ± 0.0000	0.8145 ± 0.0000	0.9031 ± 0.0000	0.9633 ± 0.0000	0.8876 ± 0.0000	0.8261 ± 0.0968
128	5	0.6492 ± 0.0000	0.8043 ± 0.0000	0.9078 ± 0.0000	0.9628 ± 0.0000	0.8861 ± 0.0000	0.8235 ± 0.1000
128	4	0.6593 ± 0.0000	0.8117 ± 0.0000	0.9012 ± 0.0000	0.9638 ± 0.0000	0.8858 ± 0.0000	0.8232 ± 0.0994
128	2	0.6444 ± 0.0000	0.8070 ± 0.0000	0.9075 ± 0.0000	0.9631 ± 0.0000	0.8857 ± 0.0000	0.8231 ± 0.1006
64	4	0.6576 ± 0.0050	0.8080 ± 0.0013	0.9052 ± 0.0045	0.9656 ± 0.0016	0.8857 ± 0.0002	0.8230 ± 0.0994
64	2	0.6528 ± 0.0066	0.8052 ± 0.0023	0.9057 ± 0.0032	0.9651 ± 0.0007	0.8855 ± 0.0004	0.8228 ± 0.0996
64	5	0.6538 ± 0.0050	0.8044 ± 0.0019	0.9058 ± 0.0037	0.9653 ± 0.0014	0.8853 ± 0.0005	0.8224 ± 0.0997
64	3	0.6520 ± 0.0067	0.8051 ± 0.0018	0.9042 ± 0.0044	0.9649 ± 0.0019	0.8853 ± 0.0011	0.8223 ± 0.0994
256	5	0.6536 ± 0.0010	0.8044 ± 0.0033	0.9036 ± 0.0042	0.9644 ± 0.0022	0.8844 ± 0.0002	0.8213 ± 0.1003
256	4	0.6434 ± 0.0000	0.8018 ± 0.0000	0.9017 ± 0.0000	0.9619 ± 0.0000	0.8823 ± 0.0000	0.8181 ± 0.1013
32	3	0.6369 ± 0.0094	0.7950 ± 0.0041	0.8977 ± 0.0032	0.9635 ± 0.0022	0.8798 ± 0.0012	0.8139 ± 0.1031
32	4	0.6384 ± 0.0037	0.7935 ± 0.0033	0.8986 ± 0.0037	0.9636 ± 0.0016	0.8799 ± 0.0009	0.8139 ± 0.1031
32	2	0.6399 ± 0.0058	0.7924 ± 0.0024	0.8983 ± 0.0033	0.9629 ± 0.0023	0.8796 ± 0.0004	0.8135 ± 0.1023
32	5	0.6350 ± 0.0077	0.7931 ± 0.0056	0.8981 ± 0.0022	0.9625 ± 0.0005	0.8792 ± 0.0011	0.8128 ± 0.1035
256	2	0.6320 ± 0.0044	0.7971 ± 0.0000	0.8939 ± 0.0034	0.9587 ± 0.0018	0.8781 ± 0.0002	0.8120 ± 0.1023

Fake-factor method uncertainties

Sources of systematic uncertainties associated with the FF method:

- Statistical uncertainties
- True τ contamination in the anti- τ CR
- α_{MJ} fitting procedure uncertainty
- Tau RNN Identification SF variation
- Heavy flavor jet fraction

Source of uncertainty	$\tau + \text{jets}$		$\tau + \ell$	
	Effect on yield	Shape	Effect on yield	Shape
Fake factors: statistical uncertainties	3.9%	✗	3.2%	✗
Fake factors: True $\tau_{\text{had-vis}}$ in the anti- $\tau_{\text{had-vis}}$ CR	+3.4% -3.2%	✗	+4% -4.3%	✗
Fake factors: tau RNN Identification SF	2.7%	✓	2.7%	✓
Fake factors: α_{MJ} uncertainty	3.6%	✗	1.9%	✗
Fake factors: heavy flavor jet fraction	6%	✓	5.53%	✓

Sources of Systematic Uncertainty

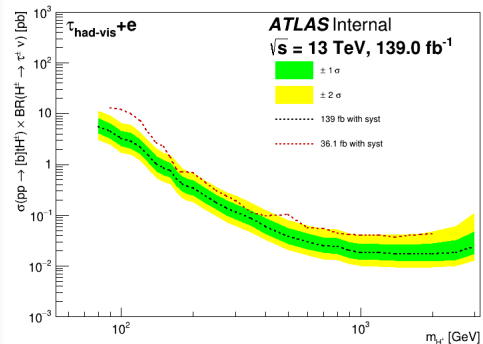
Source	Impact on the expected event yield (%)					
	τ -jets		$\tau + e$		$\tau + \mu$	
	$t\bar{t}$	$H^\pm 200 \text{ GeV}$	$t\bar{t}$	$H^\pm 200 \text{ GeV}$	$t\bar{t}$	$H^\pm 200 \text{ GeV}$
$T_{had-vis}$ reconstruction efficiency	± 1.24	± 1.22	± 1.23	$+1.22$ -1.23	± 1.23	± 1.22
$T_{had-vis}$ -id	± 1.79	± 0.52	± 1.40	± 0.50	± 1.40	± 0.48
$T_{had-vis}$ energy scale	$+2.53$ -2.80	$+2.00$ -1.66	$+1.60$ -1.44	$+1.28$ -1.66	$+1.53$ -1.39	$+1.72$ -1.46
$T_{had-vis}$ energy scale (detector)	$+1.96$ -1.55	$+1.64$ -1.49	$+0.23$ -0.21	$+1.15$ -1.08	$+0.16$ -0.55	$+0.49$ -1.5
$T_{had-vis}$ energy scale (in-situ)	$+144$ -1.43	$+0.22$ -0.74	$+1.17$ -1.20	$+0.74$ -0.63	$+1.14$ -1.15	$+0.54$ -0.37
$T_{had-vis}$ energy scale (model)	$+0.56$ -0.61	-0.06 -0.21	$+0.23$ -0.21	$+1.15$ -1.08	$+0.16$ -0.55	$+0.49$ -1.50
$T_{had-vis}$ energy scale (physics list)	$+1.27$ -1.26	-0.72 -0.65	$+0.74$ -0.65	$+0.67$ -0.25	$+0.72$ -0.63	$+0.83$ -0.60
jet uncertainties	$+7.38$ -8.39	$+6.51$ -9.06	$+3.41$ -3.31	$+4.49$ -2.78	$+3.18$ -3.24	$+3.67$ -2.96
E_T^{miss} soft term scale/resolution	$+1.31$ -1.12	$+1.15$ -1.49	$+0.29$ -0.24	$+0.88$ -0.34	$+0.30$ -0.23	$+0.21$ -0.11
trigger	$+1.23$ -1.61	± 0.03	0	0	$+0.55$ -0.56	± 56
e-id	0	0	± 0.71	± 0.73	0	0
μ -id/reconstruction/isolation	0	0	0 -0.01	0 -0.11	$+0.97$ -1.40	$+1.00$ -2.94
μ MS	0	0	0	0	$+0.09$ -0.12	$+0.40$ -0.34

Expected Yields

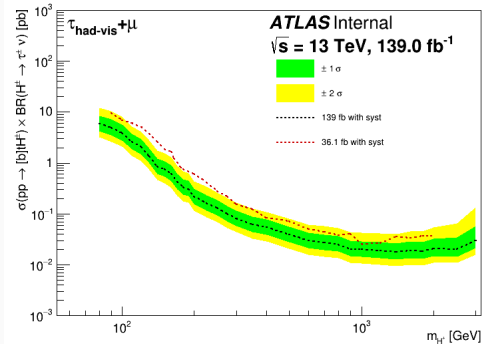
- Analysis is still blinded
 - Ongoing work with the internal ATLAS review process
- Expected number of events from each background source and two arbitrary m_{H^\pm} points
- PNN is used to separate signal from background

Sample	Event yields $+j$ -jets		Event yields $\tau + e$		Event yields $\tau + \mu$				
$t\bar{t}$	18443.27	\pm 48.35	+1545.67 -1697.11	43813.50	\pm 76.85	+1749.82 -1833.87	44486.48	\pm 75.33	+1811.78 -1907.08
Single-top-quark	2284.34	\pm 17.39	+184.69 -207.49	3260.52	\pm 20.81	+124.27 -134.66	3873.35	\pm 22.06	+158.03 -165.92
$W \rightarrow \tau\nu$	1979.17	\pm 23.63	+179.85 -229.80	2.41	\pm 0.56	+0.22 -2.15	0.07	\pm 0.12	+0.08 -0.16
$Z \rightarrow \tau\tau$	242.12	\pm 5.50	+24.27 -32.88	913.55	\pm 20.42	+64.56 -149.42	845.89	\pm 22.07	+88.71 -111.03
Diboson (WW, WZ, ZZ)	133.76	\pm 4.69	+9.47 -12.61	72.64	\pm 1.52	+5.25 -3.91	80.81	\pm 1.53	+5.40 -6.45
Misidentified $e, \mu \rightarrow \tau_{had-vis}$	328.89	\pm 6.85	+25.60 -34.58	1083.97	\pm 24.33	+41.65 -73.42	1060.30	\pm 15.84	+43.44 -70.69
Misidentified jet $\rightarrow \tau_{had-vis}$	2506.28	\pm 17.39	+130.53 -133.40	8662.43	\pm 37.49	+450.65 -470.53	8426.64	\pm 37.12	+440.04 -459.88
All backgrounds	25917.83	\pm 59.82	+1572.87 -1730.97	57809.03	\pm 93.57	+1812.82 -1846.46	58773.63	\pm 90.99	+1873.75 -1970.06
H^\pm (170 GeV), hMSSM $\tan\beta = 40$	1075.81	\pm 9.12	+82.89 -79.19	598.17	\pm 6.60	+20.84 -22.52	702.21	\pm 6.93	+22.39 -16.12
H^\pm (1000 GeV), hMSSM $\tan\beta = 40$	12910.36	\pm 59.30	+784.57 -720.17	938.90	\pm 13.25	+48.99 -37.72	1024.06	\pm 13.21	+48.42 -57.01

$H^\pm \rightarrow \tau\nu$ Expected Limits

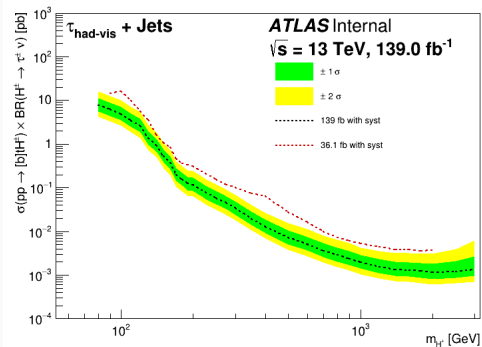


$\tau + e$

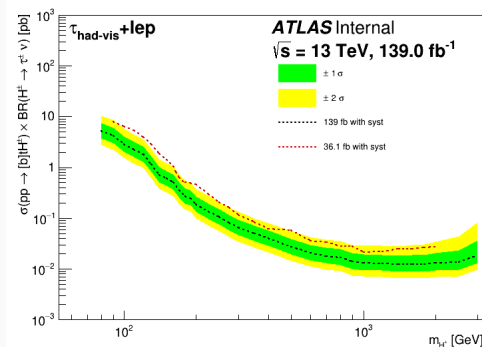


$\tau + \mu$

$H^\pm \rightarrow \tau\nu$ Expected Limits



$\tau + jets$



$\tau + \ell$